Journal of the Indian Institute of Science
Vol. 53, No. 3, July 1971

DIFFRACTION AND BACKSCATTERING OF ELECTROMAGNETIC WAVES BY CIRCULAR DIELECTRIC DISCS AT X-BAND

By M. S RAMACHANDRAIAH* AND S. K. CHATTERJEE

(Department of Electrical Communication Engineering, Indian Institute of Science, Bangalore-12 India)

(Received: February 27, 1971)

ABSTRACT

The classical Kirchhoff's theory of diffraction by a circular aperture in a conducting infinite screen is modified by taking into account the phase change introduced by the circular dielectric disc and also the effect of multiple internal reflections taking place inside the disc. The diffraction patterns thus obtained from appropriate vibration spirals and computed as function of the diameter and thickness of the disc agree well with the experimental diffraction patterns. The constructional details and characteristics of the image plane apparatus developed and used for the measurement of the diffraction patterns and back scattering cross-sections are discussed.

1. INTRODUCTION

The problem of diffraction and scattering of electromagnetic waves by dielectric discs of different shapes has assumed considerable importance due to the development of microwave optics. Theoretical solutions for this problem are based on the boundary value method employing either an integral equation approach or a set of eigen-functions to represnt the incident and scattered fields. Asymptotic series solutions are normally employed to evaluate the integral equation or the eigen-functions. This method of approach is limited by the slow convergence of the series for objects whose dimensions are large compared to the wavelength of the incident wave. The evaluation of eigen-functions by using logarithmic derivative potentials[1], perturbation technique[2], the application of Rumsey's reaction concept

* Dr. M. S Ramachandraiah is at present with the chair of Electromagnetism and Microwaves at the Federal Institute of Technology, Department Electricity, Chemin de Bellerive 16, 1007—Lau Sanne (Switzerland).

assuming volume polarisation of currents by Cohen[4], extension of Cohen's work by Stickler[5] and modified[6] geometrical optics technique developed by Keller[7] have all contributed significantly to the progress of theoretical studies of scattering and diffraction by dielectric bodies. Rigorous theoretical solutions for an infinite dielectric cylinder as a boundary value problem by Lord Rayleigh[8] and exact solution to the problem of scattering by a dielectric sphere of finite dielectric constant and conductivity by Mie[9] have, however, laid the fundamental basis for such theoretical studies.

The image plane technique developed by Kodis[10] and its modified form known as double image plane technique by Row[11], the experimental work by Wiles and Mclay[12], the measurement of diffraction fields by Severin and Baeckmann[13], the measurement of backscattering cross-section of water droplets by using an image plane slotted line section by Aden[1] have helped considerably to standardise experimental technique for the study of diffraction and scattering by dielectric bodies at *K*, *X* and *S* bands. However, information regarding experimental and theoretical investigations in the near and Fresnel zones of diffraction fields around dielectric discs, the effect of disc parameters on the distribution of diffraction fields, the back scattering cross-section of circular dielectric discs of diameters greater than a wavelength seems to be lacking.

The paper presents a report of theoretical and experimental investigations on diffraction and back scattering of microwaves at 3.2 cm wavelength by dielectric discs of diameters greater than the wavelength. The investigations include an extension of Kirchoff's theory of diffraction to the case of diffraction by circular dielectric discs, measurement and analysis of diffraction fields and backscattering cross-section of circular dielectric discs of different thickness, diameter and dielectric constant. It is hoped that the results of the present investigations will lead to a better understanding of the mechanism of electromagnetic radiation from dielectric bodies.

2. KIRCHHOFF'S THEORY

The problem of diffraction and scattering of electro-magnetic waves by obstacles and apertures requires solution of the vector wave equation in the appropriate coordinate system and the application of proper boundary conditions. Kirchhoff[14] formulated the problem of diffraction by a hole in an infinitely thin conducting screen in the form of a surface integral

$$U_p = \frac{i U_0}{4\pi} \int_{\sigma} \int \left[\frac{2\pi}{\lambda} \frac{\exp(-i\phi)}{\gamma} (1 + \cos\theta) - i \frac{\exp(-i\phi)}{\gamma^2} \cos\theta \right] d\sigma \qquad [1]$$

assuming a plane polarised monochromatic wave of wavelength λ to be incident on the aperture (Fig. 1). The amplitudes of electromagnetic field

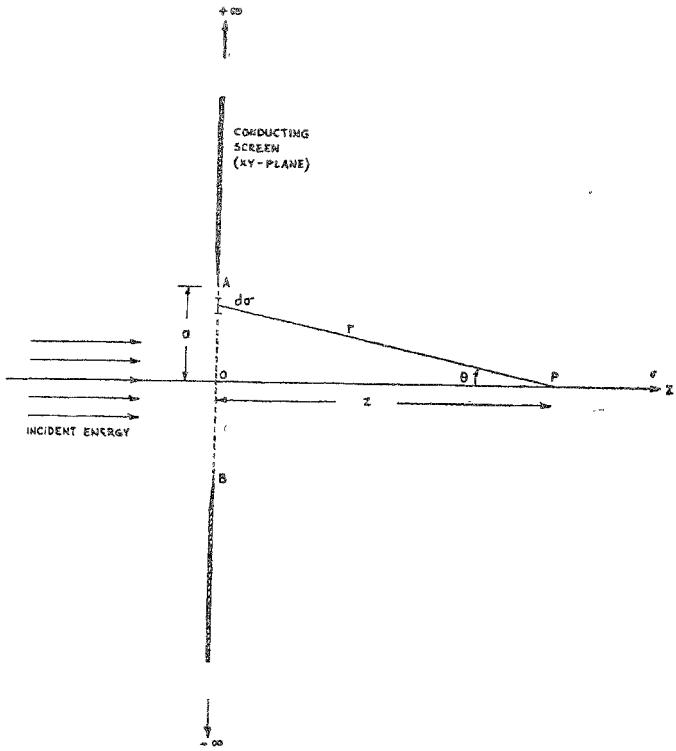

FIG. 1

Ceometry of the diffracting aperture

at the point of observation P and on the diffracting aperture are given respectlvely by U_p and U_o. The phase angle of the Huygen's wavelets at the element of area $d\sigma$ is represented by ϕ and $(1+\cos\theta)$ is the Fresnel's obliquity factor. By using proper transformations eq. [1] becomes

$$U_p = \frac{U_o i}{2} \int_0^{\beta} \left[\exp(-i\phi) \left\{ 1 - \frac{1}{(\phi + kz)} \right\} \frac{kz}{\phi + kz} + 1 \right] d\phi \qquad [2]$$

which reduces to

$$U_p = U_o\, i \left[(\sin\beta + i\cos\beta)\, \frac{\beta + 2kz}{2\beta + 2kz} - 1 \right] \qquad [3]$$

The above eq. [3] is written for the convenience of graphical representation as follows:

$$U_p = U_o\, i\, [(\sin\beta + i\cos\beta)\, \tfrac{1}{2}(1 + \cos\theta) - 1] \qquad [4]$$

where, the wave number $k = 2\pi/\lambda$ and the phase of the outermost ring of the circular aperture contributing to U_p is

$$\beta = (2\pi/\lambda)\, [\sqrt{(z^2 + a^2)} - z]$$

and

$$\cos\theta = [z/(z^2 + a^2)^{1/2}]$$

In polar coordinates, eq. [4] assumes the form

$$(U_p/U_o) = 1 - \rho \exp(-i\beta)$$

where,

$$\rho = \tfrac{1}{2}\, \{1 + [z/(z^2 + a^2)^{1/2}]\} \qquad [5]$$

The plot of real vs imaginary components of U_p/U_o for varying values of β is called the vibration spiral. The value of the real component of U_p/U_o varies between 0 and 2.0, whereas, the value of the imaginary component varies between -1.0 and $+1.0$ for different values of β, which can be varied by (i) keeping the diameter ($2a$) of the aperture constant, and changing the distance z from the origin or, (ii) keeping z constant and changing the diameter of the aperture. Fig. 2 shows a vibration spiral for fixed values of z. The diffraction patterns corresponding to a vibration spiral are obtained in the following way. The first term on the right hand side of eq. [5] represents a vector of unit length and zero reference phase. The second term represents the vector AB. The resultant vector of OA and AB is represented in amplitude and phase by OB. The term $-\exp(-i\beta)$ represents a rotating vector whose radius vector sweeps in a negative or clockwise direction. The factor $\rho = \frac{1}{2}(1 + \cos\theta)$ causes the length of the rotating vector to decrease as β increases. Thus when the vector AB is moved round, the resultant goes through maxima and minima as β passes through integral multiples of π, yielding the characteristic diffraction pattern.

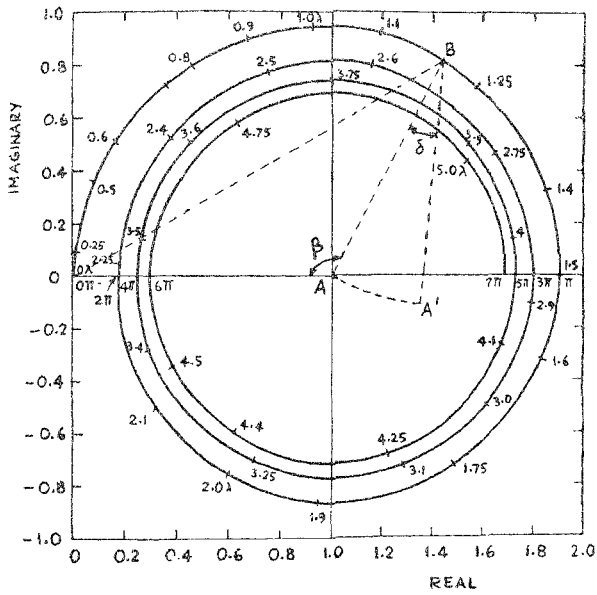

FIG. 2

Vibration spiral for diffraction at $Z=2\lambda$ along the axis for apertures of different radii. Radii of apertures are marked along the spiral

3. MODIFIED KIRCHHOFF'S THEORY

Problems of diffraction by dielectric objects are similar to corresponding problems involving conducting objects, but they are complicated by the transparency of dielectric objects to high frequency electromagnetic radiation and the presence of multiple internal reflections. The theory of diffraction by Kirchhoff is modified by taking into account (i) the phase change due to the optical path difference introduced by the dielectric object and (ii) the effect of multiple internal reflections :

(i) *Effect of Phase Change* :

If a plane polarised wave (λ) is incident on a thin homogenous isotropic lossless dielectric disc of dielectric constant ϵ_r and thickness t immersed in free space of dielectric constant ϵ_o, the optical path difference due to the presence of dielectric disc gives rise to the following phase change :

$$\delta = (2\pi t/\lambda)(\sqrt{\epsilon_r} - \sqrt{\epsilon_o}) \qquad [6]$$

The resultant electric field at P is due to two components, one of which comes from the disc and the other from the corresponding complementary sheet extending to infinity, but is displaced in phase δ with respect to that of the disc. In Fig. 2, OB represents the field behind the aperture and BA the field behind the complementary disc. BA represents the field behind the same disc when the medium surrounding the disc corresponds to a phase difference of δ with respect to that in case of field represented by BA. That is, the vector BA is rotated through an angle δ in the positive direction. Therefore, the field at P behind the disc is given by the new coordinates of BA, which when plotted in the complex plane gives the new vibration spiral (Fig. 3). The diffraction pattern corresponding to the new spiral is obtained in the usnal way.

(ii) *Effect of internal reflections* :

Multiple internal reflections of electromagnetic waves at the twowalls of the dielectric disc will introduce further phase displacement which can be taken into account by considering the theory of multiple beam interference[15,16]. When a vertically polarised wave is incident normally on the disc, the transmitted electric filed E^t is given in terms of the incident electric field E^i, by the following relation :

$$E^t = \left[\frac{\tau\tau'}{1 - r^4 \exp(i\Delta)}\right] E^i \qquad [7]$$

where, the phase difference Δ due to internal reflection is

$$\Delta = 2(2\pi/\lambda_0)\, t\sqrt{\epsilon_r} \qquad [8]$$

and τ and τ' represent the transmission coefficient for a wave travelling from air to plate and from plate to air and r is the reflection coefficient for a wave travelling from air into plate.

The normalised amplitude and the phase of the transmitted electric field are respectively given by

$$|E^t/E^i| = \frac{2n}{[4n^2 + (1-n^2)^2 \sin^2 \tfrac{1}{2}\Delta]^{1/2}} \qquad [9]$$

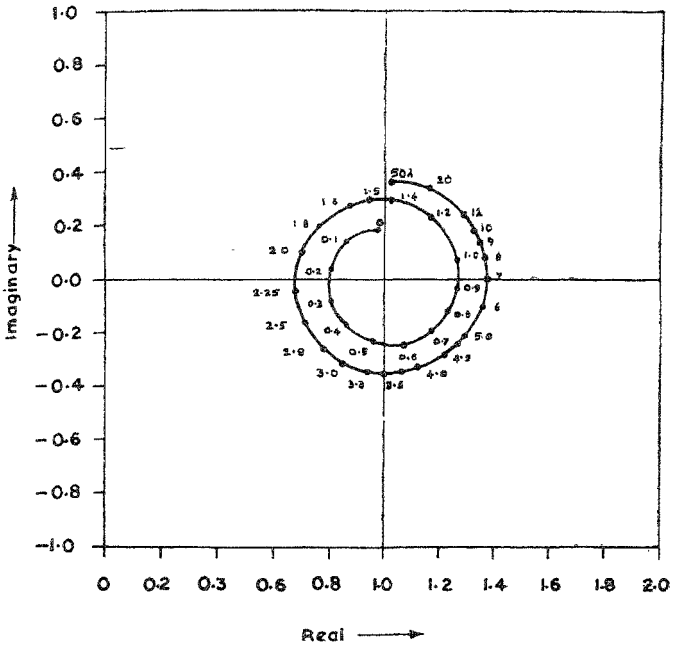

FIG. 3

Vibration spiral for axial diffraction by a circular perspex disc $r=3.2$ mm $D=4\lambda$
Distances along the disc axis are marked along the spiral

$$\text{and} \quad \phi = \arctan\left[\frac{(1-n)^2 \sin \Delta}{(1+n)^2 - (1-n)^2 \sin \Delta}\right] \qquad [10]$$

The effect of multiple internal reflection is taken into account by using the new value of the field given by eqns. [9] and [10] in plotting the vibration spiral (Fig. 4).

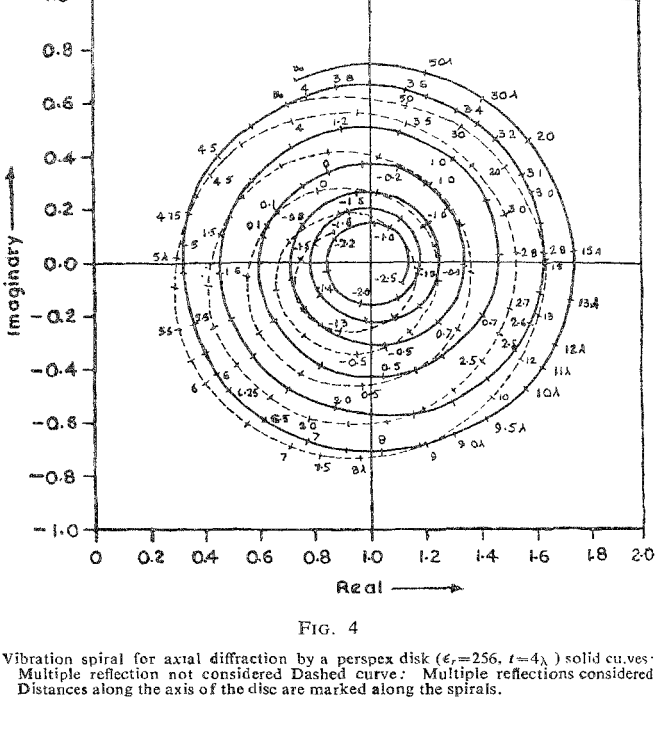

FIG. 4

Vibration spiral for axial diffraction by a perspex disk ($\epsilon_r=2.56$, $t=4\lambda$) solid curves: Multiple reflection not considered Dashed curve: Multiple reflections considered Distances along the axis of the disc are marked along the spirals.

4. BACKSCATTERING CROSS SECTIONS

The back scattering cross section σ_B of an obstacle is given by the well known definition[17].

$$\sigma_B = \frac{P^S(\text{isotropic})}{S^i} = \lim_{r\to\infty} 4\pi r^2 \left|\frac{E^s}{E^i}\right|^2 \qquad [11]$$

The back scattering cross section depends on the shape, size, material of the obstacle, wavelength, polarisation and the shape of the wavefront of the incident field. The theory of backscattering by dielectric discs of

diameters greater than a wavelength has not been worked out, however it was thought worthwhile to determine σ_B of dielectric discs experimentally and correlate the results with σ_B for conducting discs of same diameters which is given by[17,18]

$$\sigma_B \text{ (metal disc)} = \pi a^2 (ka)^2 \qquad [12]$$

The backscattering cross section plotted as a function of disc diameter in a log-log graph paper yields a straight line of slope 4 (Fig. 5). The experimental determination of σ_B for dielectric discs showed also a fourth power dependence on the disc radius, but σ_B (dielectric disc) differed from σ_B (metal disc) by a constant factor equal to the reflectivity R of the dielectric material given by

$$R = \left| \frac{E^r}{E^i} \right|^2 = \frac{(1-n^2)^2 \sin^2 \frac{1}{2}\Delta}{4n^2 + (1-n^2)^2 \sin^2 \frac{1}{2}\Delta} \qquad [13]$$

where, $n = \sqrt{\epsilon_r}$ and E_r, E_i represent the amplitudes of the reflected and incident electric fields respectively.

5. Theory of Measurement of Backscattering Cross Section

The standing wave ratio method developed by King[19] is used to determine σ_B which is given by

$$\sigma_B = \operatorname*{Lim}_{l \to \infty} 4\pi l^2 |\Gamma|^2 \qquad [14]$$

where,

$$|\Gamma| = \left[\frac{S_{\pm} - 1/[1 \mp \Delta/(1-W^2)]}{S_{\pm} + 1/[1 \pm \Delta/W_2]} \right] W_2/(1-W_2) \qquad [15]$$

where, W_1 = position of voltage maximum

W_2 = position of voltage minimum

l = distance between the source and the obstacle in cm.

$\Delta = |W_1 - W_2|$ in cm.

When $W_1 > W_2$, the S.W.R. is denoted by $S = S_+$ and $|\Gamma|$ is given by eq. [15] with upper signs. But when $W_1 < W_2$, $S = S_-$ and $|\Gamma|$ is given by the same equation with lower signs.

6. Image Plane Diffraction Apparatus

Fig. 6 shows a sketch of the image plane apparatus. The image plane formed by 0.125" thick duralumin sheet is of dimension $15\lambda \times 86\lambda$ at $\lambda = 3.2$ cm.

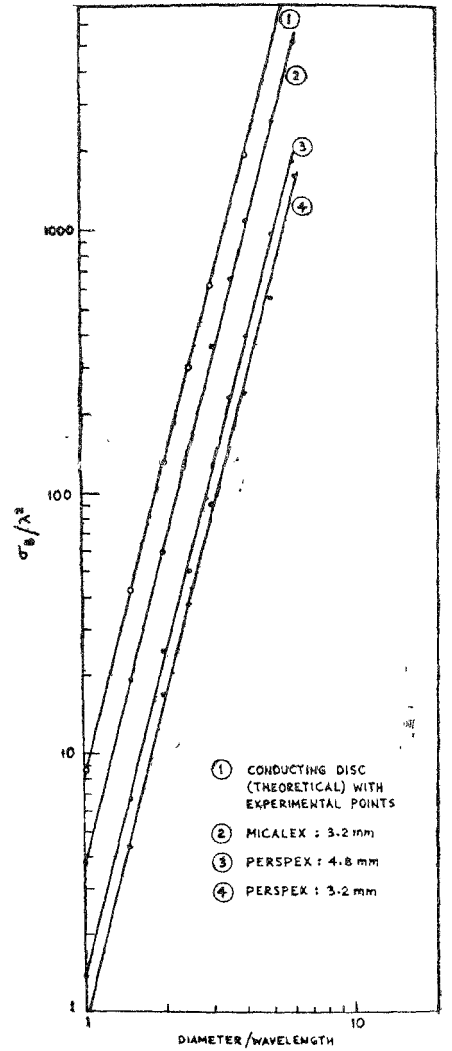

FIG. 5

Backscattering cross section as a function of disc diameter.

The sheets are mounted at a height of 6 ft from the ground level on top of a rigid wooden structure. The set *B* is fixed to the wooden frame and the other set *A*, and *C* is movable. Panels *A* and *C* can be moved in two mutually perpendicular directions on smooth aluminium angles in the grooves formed by the fixed panels *B*. Panel *A* is 9 feet × 3 feet and carries a half pyramidal horn *E* at one end and the diffracting object I at the other. The horn illuminates the object uniformly. The transverse narrow panel *C* is 6 inches wide and 9 feet long It carries a probe *G* at its center and can be moved across the image plane (parallel to the narrow sides) with the help of a rack and pinion attachment mounted at the bottom of image plane.

Separation between the horn and the probe (*E* and *G*) can be increased by sliding the source panel away from the probe, keeping the separation between the source and the obstacle (*I*) constant. The resulting air gap in the image plane is filled up by duralumin inserts (.125" thick × 3 feet long). The inserts have been made with widths which increase from 0 5 λ to 20.0 λ in steps of half a wavelength. These inserts are accurately milled to fit in flush with the rest of the image plane. For axial field and backscattering cross section measurements the image plane slotted line section can be fitted in place of inserts. The inserts or the slotted line section are prevented from sagging by fixing a plywood sheet at the bottom of the image plane.

All equipments and components except the obstacle, half horn and the probe protruding through the slot are located below the image plane. The isolation of the observer and all equipments from the observed fields makes it possible to obtain reliable field measurements.

7. Probe Assemblies

The requirements to be fulfilled by the probe for the measurement of near and Fresnel Zone fields are given by Richmond and Tice[20]. The length of the monopole probe that proved satisfactory for the measurement of transverse diffraction patterns was 0.25 λ made of 20 SWG copper wire. The transverse probe protrudes into the diffraction field space above the image plane through a 0.125" diameter circular hole drilled in the center of the transverse probe panel. The probe is connected to a crystal tuner the output of which is applied to a high gain detector amplifier. The span of movement of the probe assembly is 90 cms across the image plane. The probe is moved by means of a Vernier attachment.

The axial probe assembly (Fig. 7a and 7b) is employed to measure the shadow-zone axial fields and backscattered fields. This probe is also a monopole of length 0 25 λ and is fitted in a slotted line section.

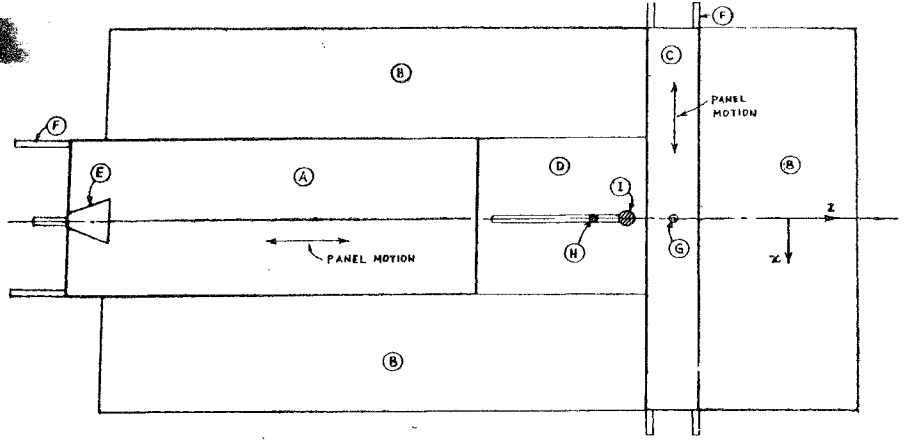

(A) SOURCE - PANEL.
(B) FIXED CONDUCTING SHEET.
(C) PROBE-PANEL
(D) SLOTTED-PROBE PANEL.
(E) ILLUMINATING HORN
(F) IRON-ANGLES ON WHICH THE PANELS SLIDE
(G) TRANSVERSE PROBE
(H) AXIAL PROBE IN THE SLOT
(I) OBSTACLE

PLAN

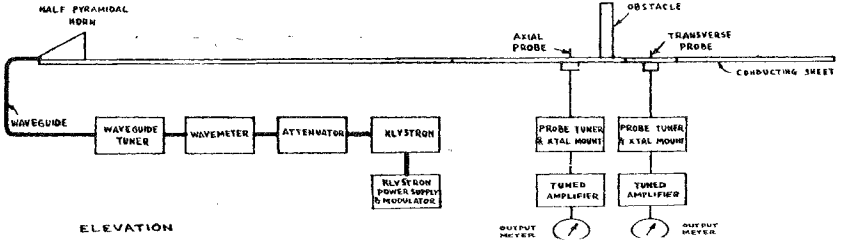

ELEVATION

FIG 7a
A bottom view of the image-plane slotted section and probe assembly

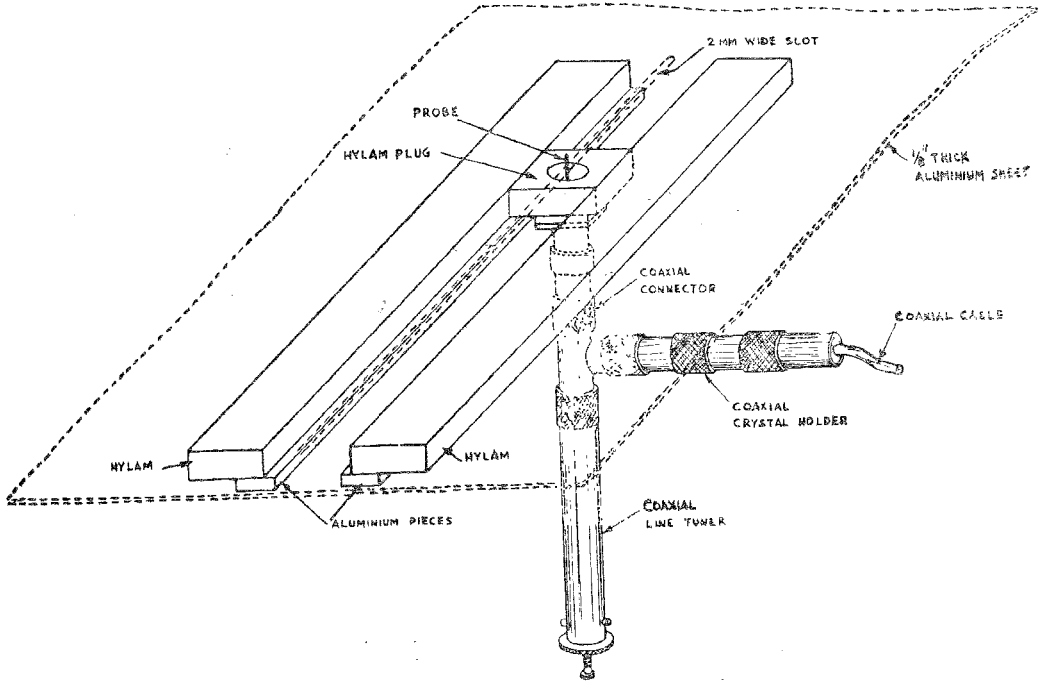

FIG. 7b

Image plane slotted line and probe assembly.

8. IMAGE-PLANE SLOTTED LINE SECTION

The general considerations which guide the design of a conventional waveguide slotted line section such as high mechanical precision, low field distortion and uniformity of motion of the probe have been taken into account in designing the image plane slotted line section, which is constructed out of a $3' \times 3' \times 0.125''$ plane.duralumin sheet. A slot 50 cm long and 2 mm wide is milled along its centre line. The probe with its associated coxial connector is mounted in $2.5'' \times 1.5'' \times 0.5''$ plug of a hard dielectric material. The plug's longer sides were milled parallel to each other and polished to a high degree of smoothness. This plug with the probe moves smoothly in a guiding groove formed by two $22'' \times 1.5'' \times 0.5''$ sized dielectric strips of the same material. The guiding walls of these strips were also milled and polished to smoothness. The dielectric plug with the probe holder moves on two $20' \times 1'' \times 0.25''$ sized polished aluminium strips attached to the dielectric strips that form the sides of the guiding grove. To minimise the disturbances caused by the slot, the groove in which the probe rides, is constructed in the form of half wavelength cavity with respect to the slotted plane. A short circuit formed at the bottom of this cavity is effectively transformed to a short circuit in the plane of the slot. When mounted on the image plane the slot of the slotted line coincides with the horn axis.

9. PERFORMANCE OF THE DIFFRACTION APPARATUS

In evaluating the performance characteristics of the diffraction apparatus the following aspects are considered ; (i) uniformity of illumination of the diffracting object and (ii) symmetry of diffraction pattern.

To evaluate the uniformity of illumination, transverse electric field intensities were recorded on the image plane for different separations between the horn and the probe. For a distance greater than 100 λ from the horn, the H plane illumination was uniform within $\pm 5\%$ of the maximum intensity. Over a span of more than 12 λ. A direct evaluation of the uniformity of phase distribution could not be made. The uniformity of illumination has also been evaluated indirectly by conducting experiments on standard objects like cylinders conducting spheres and discs. A comparison of the experimental results obtained on this diffraction apparatus for a dielectric cylinder with the results published by Wiles and McLay[21] and the curve computed with the aid of the theory given by Wait and Froese[22] is shown in Fig. 8. The following Table 1 gives the results of the measurement of σ_B of conducting spheres. The experimental values of σ_B are compared with the theoretical values of Mentzer[23]. It can be seen from data in Table 1 that the results agree well with the already published results or other authors.

TABLE 1

Backscattering cross sections of conducting spheres $\lambda_0 = 3.2$ cm.

Radius of the sphere (cms)	Theoretical cross sections (in λ^2) Ref. 23	Experimental cross section (in λ^2)
3.6	3.55	3.13
5.0	7.65	8.9
8.0	10.6	18.2

The results of backscattering cross sections of conducting discs agree within $\pm 5\%$ of the theoretical values. It may therefore be assumed that the performance of the diffraction apparatus is fairly satisfactory.

10. Diffraction and Scattering Measurements

The electric field E_y is polarised in a direction (y) perpendicular to the image plane ($x-z$), the horn axis being in the z-direction. It is assumed that the polarization of the electric field of the scattered field is the same as that of the incident electric field. The diffracted field intensities E_y observed in the presence of the obstacle are normalised with respect to the incident field intensities E_0 observed at the same points in the absence of the obstacle. The relative intensities are plotted as ordinates against normalised distance along abscissa. In these patterns unity in the ordinate corresponds to incident elecrric field intensity.

11. Shadow Zone Axial Diffraction Patterns

The axial diffraction patterns are determined with the aid of the axial probe assembly. The half circular dielectric disc is mounted between the horn and the travelling probe. The disc rests on its diameter symmetrically across the slot (Fig. 9). The disc is illuminated with microwave power and the probe is moved in the slot in the shadow regions of diffraction. The probe output indicated by the detector amplifier current is noted corresponding to each position of the probe. The disc is removed and the incident field intensity is noted under the same working condition. Fig. 10 shows some of the shadow zone axial diffraction patterns.

The variation of the field intensity at a fixed distance behind the diffracting disc has also been studied for $z = 1\ \lambda$, $2\ \lambda$ and $3\ \lambda$ as a function of disc thickness and diameter. Fig. 11 shows the patterns for $z = 1\ \lambda$.

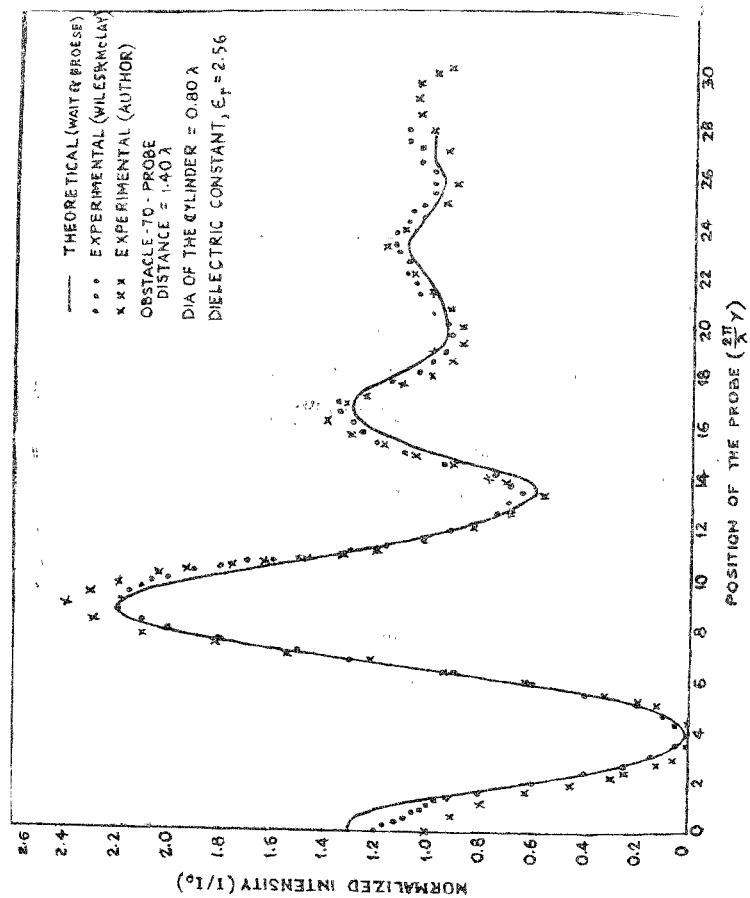
THEORETICAL (WAIT & PROBE)
EXPERIMENTAL (WILES & McLAY)
EXPERIMENTAL (AUTHOR)
OBSTACLE-TO-PROBE DISTANCE = 1.40 λ
DIA OF THE CYLINDER = 0.80 λ
DIELECTRIC CONSTANT, ϵ_r = 2.56
NORMALIZED INTENSITY (I/I$_0$)
POSITION OF THE PROBE ($\frac{2\pi}{\lambda}$Y)
0
0.2
0.4
0.6
0.8
1.0
1.2
1.4
1.6
1.8
2.0
2.2
2.4
2.6
2
4
6
8
10
12
14
16
18
20
22
24
26
28
30

FIG 9
A perspex disc mounted on the image-plane slotted section.

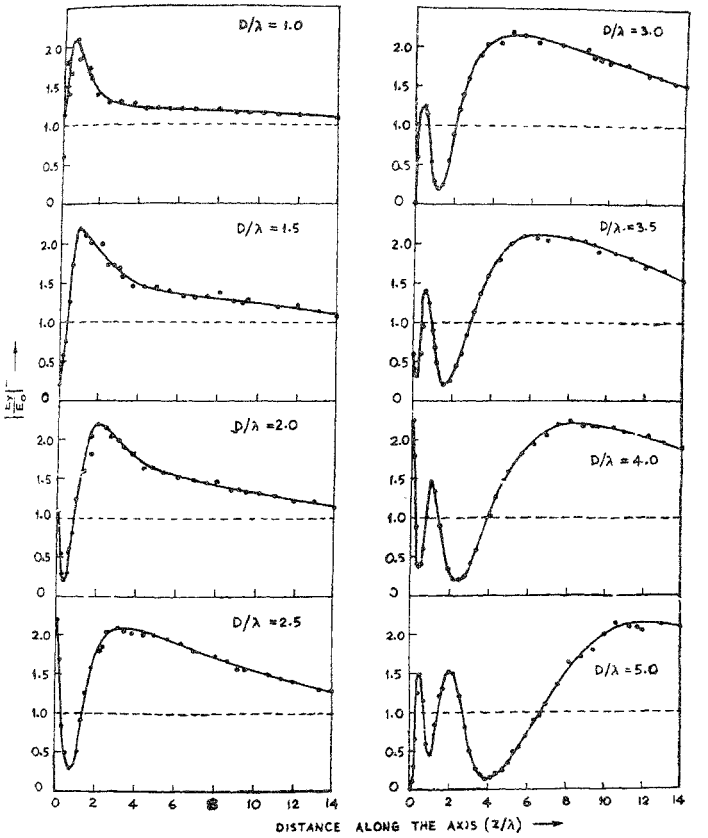

FIG. 10

Shadow zone axial diffraction patterns. Perspex discs t=3.2 mm.
The dotted line indicate the incident field intensity level

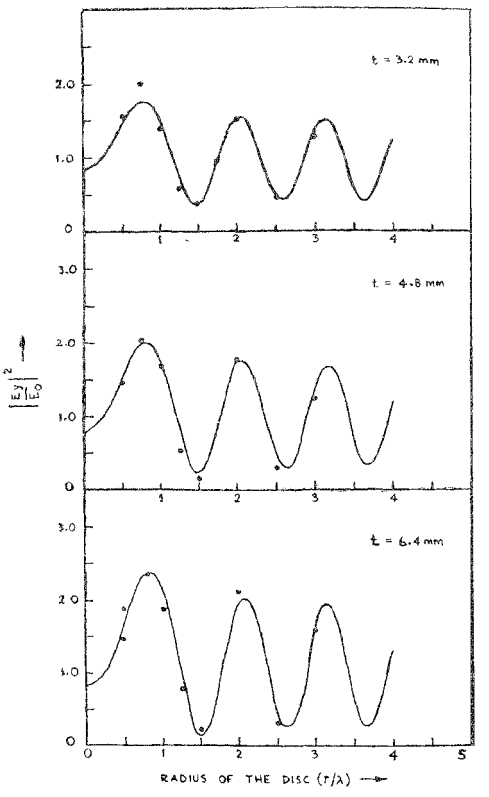

FIG. 11

Shadow zone field intensities at a distance of $z=1\lambda$ on the axis of a persfex disc as a function of disc radius.

— Theoretical
. . Experimental

12. Transverse Diffraction Patterns

The transverse diffraction patterns (Fig. 12 and 13) show the nature of near and Fresnel zone fields behind the diffracting discs. The nature of transition of transverse fields from near zone to the far zone of the diffraction patterns of a perspex disc of thickness 6.4 mm and diameter $=4\lambda$ has been studied from $z/\lambda=1.0$ to 15.0 in steps of $z/\lambda=0.5$ and some of the results are shown in Fig. 14.

The effect of the dielectric constant of the material of the disc on the nature of transition of fields from near to the far zone of the diffracted field has also been studied from $z/\lambda=1$ to 10. Some of the results are reported in Fig. 15 which shows a comparison of patterns for discs of different dielectric constants but of equal diameter and thickness.

Fig. 16 shows an interesting feature of the problem of diffraction by dielectric discs. The diffraction pattterns of two circular discs of equal diameter but of different dielectric constants and physical thickness, but having same optical thickness are compared. Perspex ($\epsilon_r=2.56$) disc of $t=6.4$ mm offers a phase delay of 45° and Hylam ($\epsilon_r=4.2$) of $t=3.2$ mm. introduces a phase delay of 42° at $\lambda=3.2$ cms.

13. Backscattering Cross Sections

The obstacle is mounted on the slotted line leaving sufficient length of the slot free for the axial probe to travel between the horn and the obstacle. When the obstacle is illuminated by microwave power from the horn, the resulting standing wave pattern between the incident and backscattered fields is measured by moving the probe along the slot. The maxima and the minima are recorded at different positions along the slot and hence the v.s.w.r. is determined. The average backscattering cross section is calculated by using eq. [11]. The backscattering cross section of dielectric and conducting discs as functions of disc diameter are plotted (Fig. 5) on a log-log paper. The theoretical values of σ_B for metal discs are calculated from eq. [12].

14. Discussion

(a) *Shadow zone axial diffraction pattern* :

Some of the interesting features observed from the axial diffraction patterns (Fig. 10 and similar figures for different thickness $t=4.8$ mm, 6.4 mm, etc.) are :

(i) A pronounced maximum appears in the shadow zone along the axis of the disc.

(ii) The maxima and minima of the electric field occur in the plane of the disc.

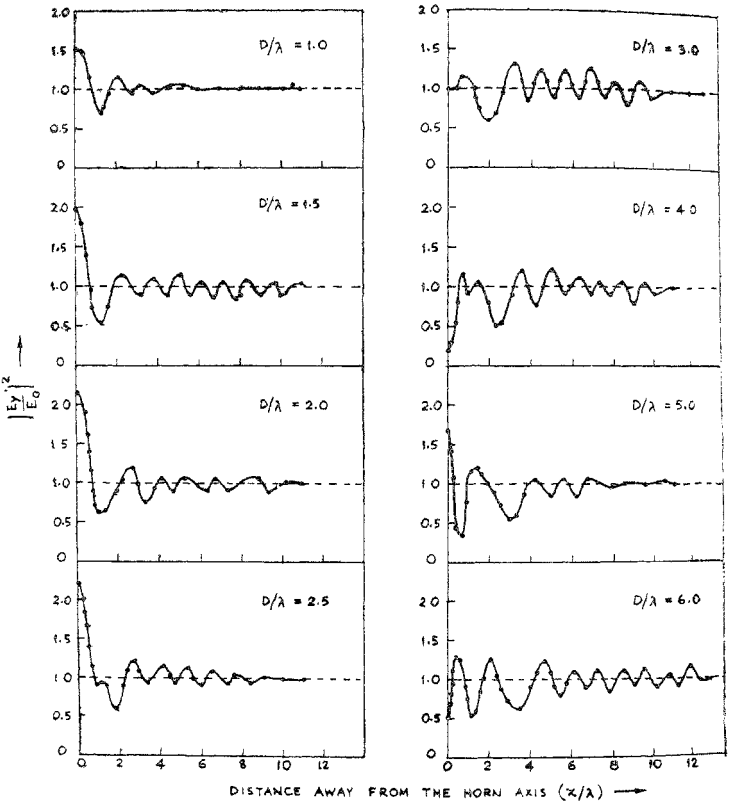

FIG. 12

Transverse diffraction patterns perspex discs, t=6.4 mm, z=2λ. The dotted lines indicate the incident field intensity level.

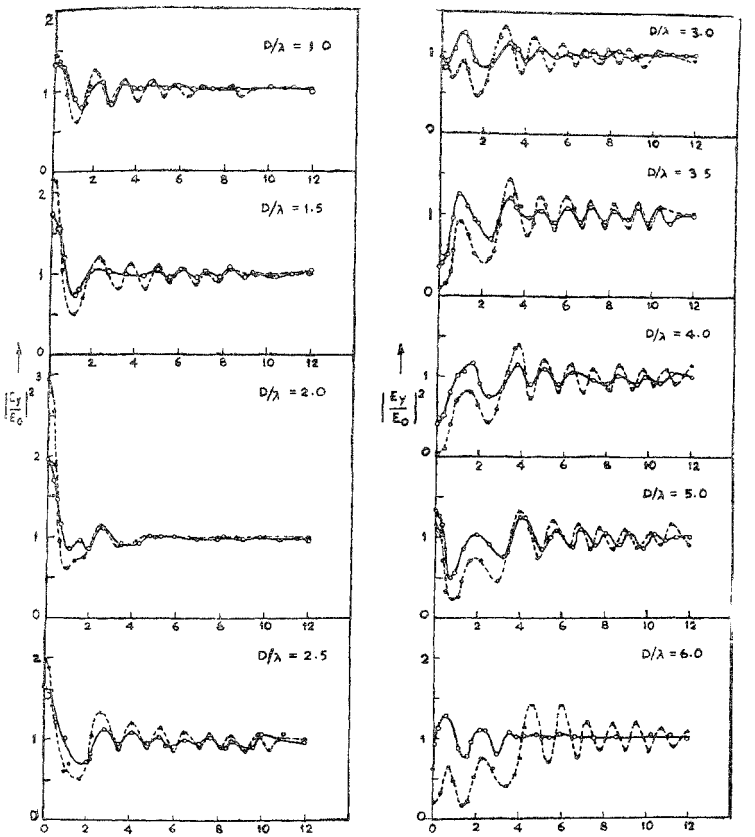

FIG. 13

Comparison of near zone transverse diffraction patterns of two different dielectric discs of 3 2 mm thickness ($z=2\lambda$).
. . Micalex -o-o- Perspex.

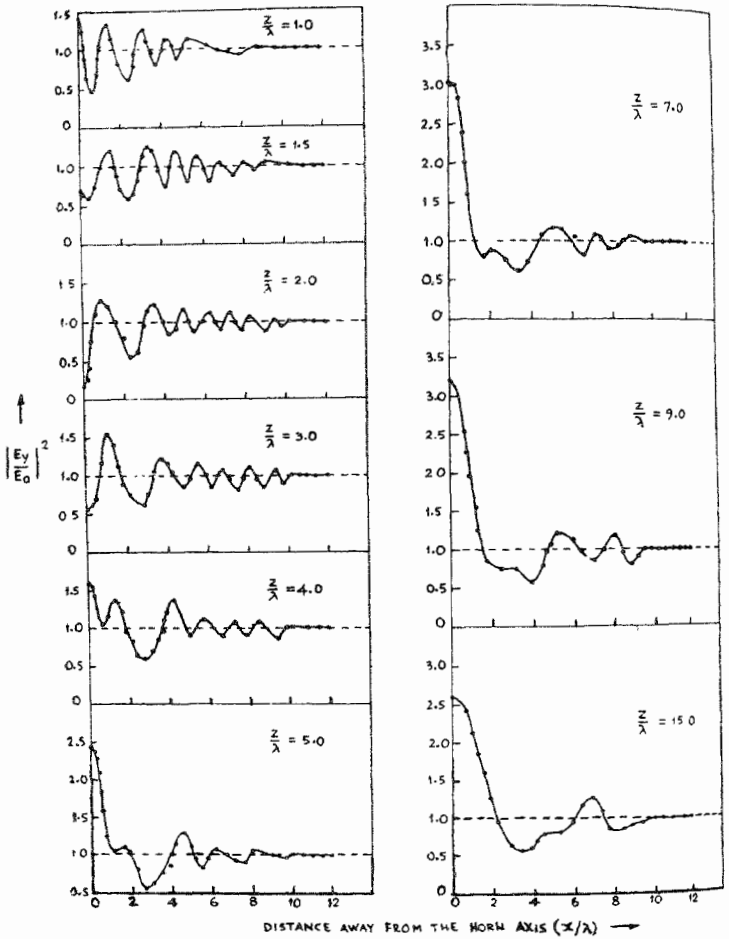

FIG. 14

Transverse diffraction patterns in different planes behind the perspex disc $D=4\ \lambda$, $t=6.4$ mm. The dotted lines indicates the intensity field intensity level

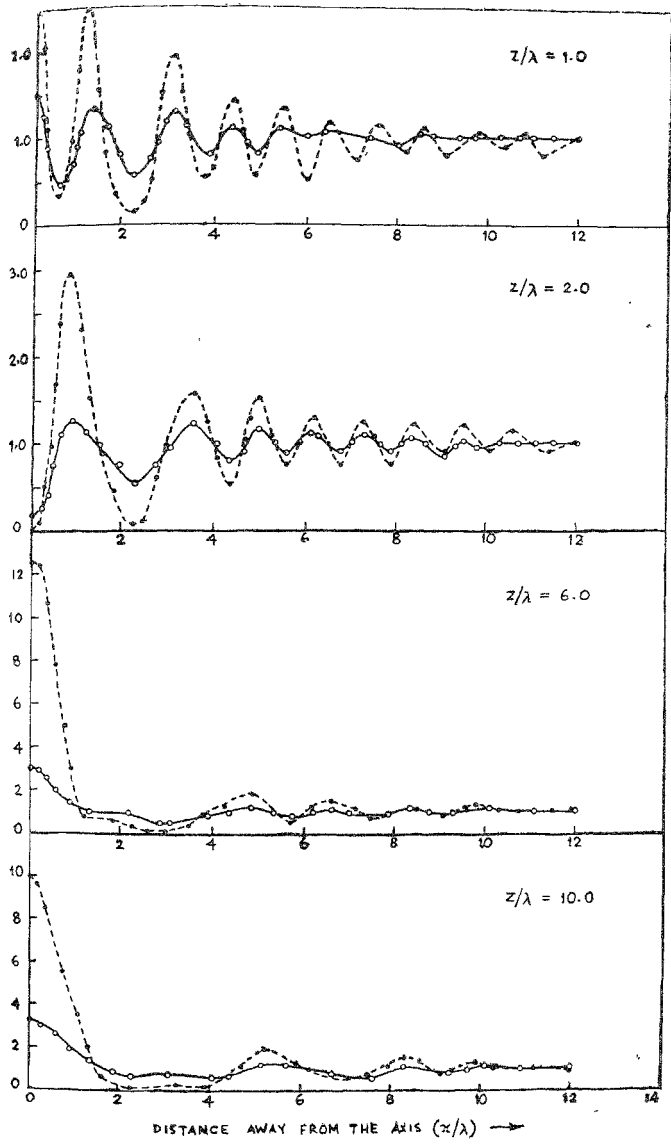

FIG. 15

Comparison of transverse diffraction patterns of two different dielectric discs
(D=4 λ, t=6.4 mm.)
—.— Micalex -o-o- Perspex.

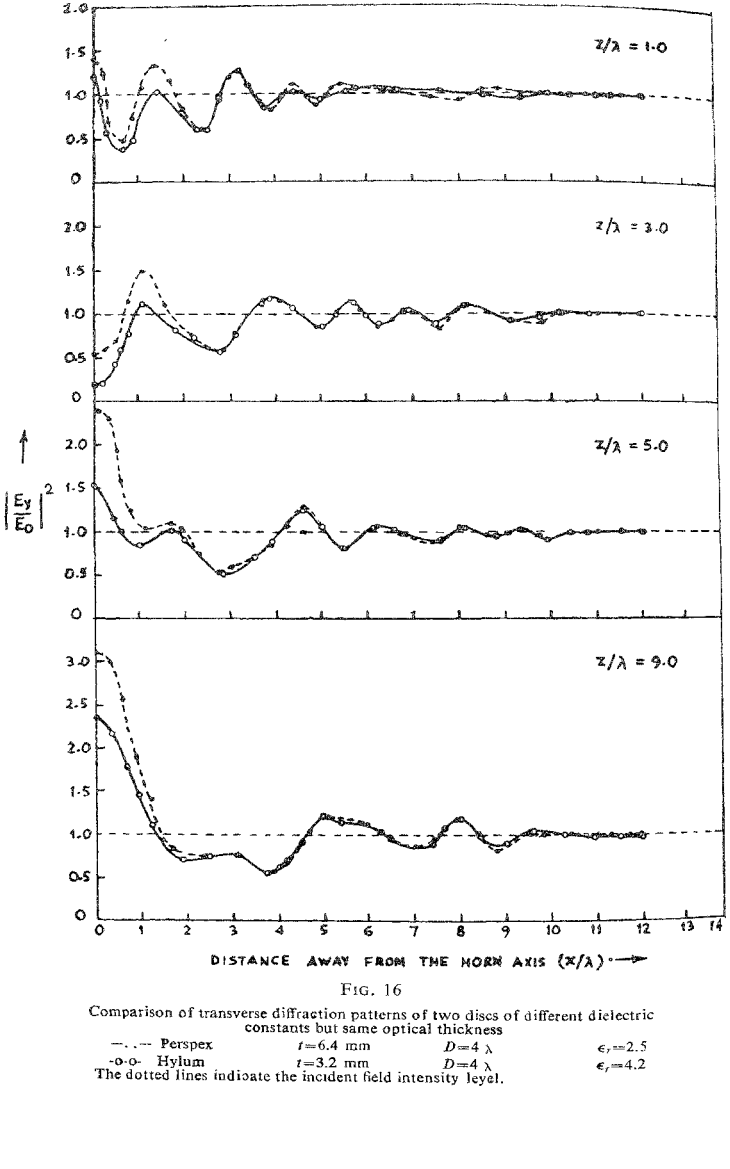

FIG. 16

Comparison of transverse diffraction patterns of two discs of different dielectric constants but same optical thickness

—·—·— Perspex t=6.4 mm D=4 λ ϵ_r=2.5

-o-o- Hylum t=3.2 mm D=4 λ ϵ_r=4.2

The dotted lines indicate the incident field intensity level.

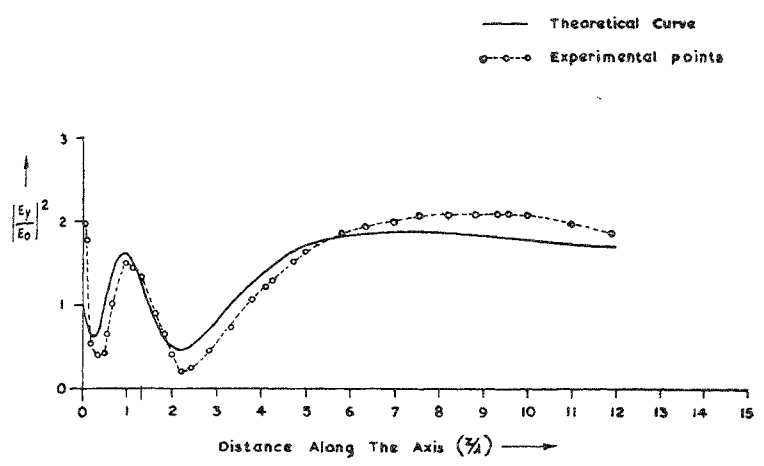

FIG. 17*a*

Axial diffraction pattern of a perspex circular Disc (ϵ_r=2.56, t=3.2 mm, D=4.0λ .)

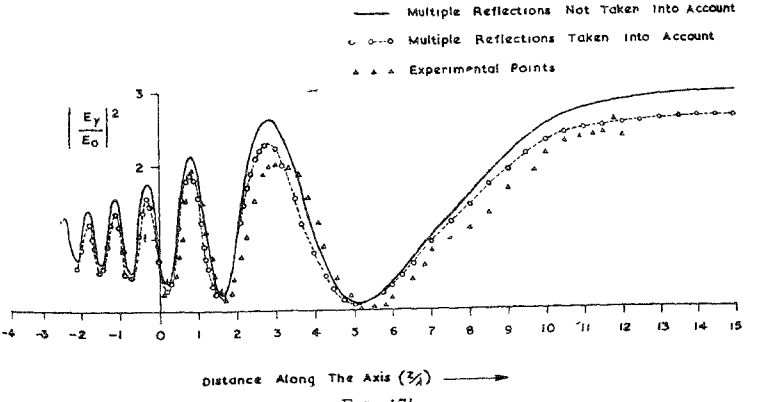

FIG 17*b*

Axial Diffraction pattern of a perfex circular Disc t=6.4 mm, Dia=6.0 λ ($\delta = 3^0$)

(iii) The number of maxima and minima occurring along the axis remain the same for a disc of a given diameter irrespective of its optical thickness. These extrema occur essentially at the same positions. The intensities of these patterns vary according to their optical thickness.

(iv) The number of maxima and minima appear to be equal to D/λ, where D is the diameter of the disc in wave-lengths.

(v) A comparison between theoretical and experimental results of axial diffraction patterns for perspex discs is shown in Fig. 17. The theoretical patterns are obtained from the vibration spirals shown in Figs. 3 and 4 respectively. The plots show that Kirchhoff's theory can predict fairly satisfactorily the positions of the maxima and minima of diffraction patterns. Values of Theoretical intensities of these extrema are also nearly same as those observed experimentally.

(vi) It is observed from Fig. 11 (and other similar figures for $z=2\lambda$ and $z=3\lambda$ which are not reported) that the diffracted field intensities in the near field region vary in a periodic manner. The peak intensity falls off gradually as the radius of the disc is increased. This can be explained on the basis of Frensel zone theory. From Fig. 2 it is observed that an increase in the radius of the aperture corresponds to exposing increasing number of Frensel zones that contribute to the varying phase relations at a particular point of observation on the axis. This results in the occurrence of successive maxima and minima.

(vii) For a fixed distance behind the disc, the maxima and minima occur at the same position for discs, of equal radii, irrespective of their optical thickness. Increased optical thickness results in the increase of intensity of the maxima and a decrease in intensity of the minima.

b) *Transverse diffraction patterns* :

(i) Fig. 16 shows that the patterns for the two discs of same optical thickness in each of the transverse planes are identical both in positions and intensities of the extrema, except for the intensity of the first extremum nearest to the disc axis. All these patterns show that the disc with greater physical thickness (perspex) yields large relative intensities near its axis than the disc with smaller physical thickness. Except for this difference, the diffraction patterns may be considered to be identical. This apparent discrepancy in itensities has not been reported earlier by any author. It appears that for the development of a satisfactory theoretical solution to the problem, the behaviour of electromagnetic fields

near the dielectric edges of finite thickness has to be understood. This aspect of the problem does not appear to have received attention from the workers in the field.

(ii) Sharp maxima and minima characteristics of the near field regions are observed from the transverse diffraction patterns (Fig. 12). The number of these maxima and minima occurring in any transverse plane in the near field increase in number with increasing disc diameter. It has been observed by Ehrlich *et. al*[24] that for an aperture in a conducting screen, the number of maxima and minima in the H-plane of the aperture is equal to n when the aperture diameter is equal to $n\lambda$ (n is an integer). But no such general law could be established in the case of dielectric discs due to the complicated phase and coordinate relations in the near field of the obstacle.

(iii) The dielectric constant has pronounced effects on the intensity of the pattern but no appreciable influence is observed on the nature of the pattern (Fig 13).

(iv) The nature of transition of transverse fields from the near to the far zone region of dielectric disc (Fig. 14) shows a gradual development of focussing action after $z=3\lambda$. As the distance is further increased, the major lobe along the axis gain in intensity at the expense of side lobes which diminish progressively both in number and intensity. With increasing distance from the disc, the major lobe grows and broadens but continues to absorb the side lobes. At $z=15\lambda$ which is almost the far zone of the disc, there is only one major lobe and well separated minor lobes.

(v) Fig. 15 furnishes further additional information regarding the influence of dielectric constant on the nature of transverse fields in various zones of diffraction fields. It is observed that for each separation of the disc, the extrema of the patterns coincide almost exactly, but intensities change in a pronounced manner.

(c) *Backscattering Cross Section*:

Fig. 15 shows that σ_B for circular dielectric disc of diameters greater than a wavelength varies as the fourth power of the disc diameter as is the case for for conducting discs. It is found that σ_B for a dielectric disc of given thickness and dielectric constant differs from the theoretical value of σ_B for conducting disc of corresponding diameter by a constant factor which is empirically found to be equal to reflectivity R of the dielectric disc (eq. 12). The theoretical and experimental values of σ_B for perspex discs of $t=6.4$ mm are given in Table II. Theoretical value have been computed by multiplying the theoretical values for conducting discs by the reflectivity of the dielectric discs calculated from eq. [12]. The reflectivity $R=0.163$ for perspex discs of thickness $t=6.4$ mm.

TABLE 2

Backscattering cross section of perspex discs (ϵ_r=2 56, t=6.4 mm) R=0.163

Disc diameter D (in λ)	(Conducting disc) Theoretical eq. 12 (in λ^2)	(Perspex disc) Theoretical (in λ^2)	(Perspexdisc) Experimental (in λ^2)
1.0	7.75	1.25	1 0
1.5	39.2	6.4	5 8
2.0	124 0	20 2	22.0
2.5	302.7	49.5	47.0
3.0	628 0	102.4	106.0
3 5	1163.0	190.0	...
4.0	1984.0	324.0	318 0
5.0	4845.0	790.0	805 0
6.0	10046.0	1640.0	1597.0

CONCLUSION

The results of the present investigations lead to the following main conclusions :

(i) Kirchhoff's theory can be extended to calculate the shadow zone axial diffraction patterns of thin lossless circular dielectric discs, fairly satisfactorily.

(ii) The effect of multiple internal reflections in a dielectric disc is essentially to change the field intensity but not the nature of the diffraction patterns.

(iii) Two dielectric discs of different dielectric constants and physical thicknesses but of equal optical thicknesses yield identical diffraction patterns, except near their axes, where the intensities of the extrema differ.

(iv) Backscattering cross-sections of dielectric discs of diameter greater than a wavelength vary as the fourth power of diameter as is the case with conducting discs.

(v) Backscattering cross-section of a dielectric disc differs from that of a conducting disc of equal diameter by a constant factor equal to its reflectivity.

References

1. Aden, A. L. . . . . *J. Appl. Phys.*, 1951, **22**, 601.
2. Yen, C. . . . . *Phy. Rev*, 1964, **135A**, A1193.
3. Ramsey, V. H. . . . . *Phy. Rev*, 1954, **94**, 1483.
4. Cohen, M. H. . . . . *IRE Trans*, 1955, AP-3, 193.
5. Stickler, D. C. . . . . *Ibid*, 1958, AP-6, 148.
6. Komyomjian, Peters Thomas . . *IEEE, Trans.*, 1963, AP-11, 690.
7. Keller, J. B. . . . . *J. Opt. Soc. Amer.*, 1962, **52**, 116.
8. Lord Rayleigh . . . . . *Phil. Mag.*, 1881, **12**, 81.
9. Mie, G. . . . . *Ann. Physik*, 1908, **25**, 377.
10. Kodis, R. D. . . . . *J. Appl. Phys.*, 1952, **23**, 249.
11. Row, R. V. . . . . *Ibid*, 1953, **24**, 1448.
12. Wiles, S. J. and Mclay, A. B. . *Can. J. Phys.* 1954, **32**, 372.
13. Seveerin, H. and Backmann, W. . . *Z Ang Phys*, 1951, **3**, 22.
14. Bouwkamp, C J. . . . . *Repts. of Prog. Phys.*, 1954, 31.
15. Born, M. and Wolf, E. . . Principles of optics, 1959, **322**, 61, published by Pergaman Press, London.
16. Jordan, E. C. . . . . Electromagnetic waves and radiating systems, 1954, 141, published by Prentice-Hall.
17. King, R. W. P and Wu. T T. . . The Scattering and diffraction of waves, 1959, **131**, 144, published by the Harward Univ. Press, Cambridge, Mass.
18. Meixner, J. and Andrejewski, W. . . *Ann. d. Physik*, 1950, **7**, 157.
19. King, D. D. . . . . *Proc. IRE*, 1949, **37**, 770.
20. Richmond, J. H. and Tice, T. E. . . *IRE Trans. MTT-3*, 1955, 32.
21. Wiles, S. J. and McLay, A. B. . . *Can. J. Phys.*, 1954. **32**, 372
22. Wait, J. R. and Froese, C. . . *Can. J. Phys.*, 1954, **32**, 775.
23. Mentzer, J. R. . . . . 'Scattering and Diffraction of radio waves' 1955, 79, publisoed by Pergaman Press, N. Y.
24. Ehrlich, M. J. Silver, S. and Held, G. . . *J. Appl Phys.*, 1955, **26**, 336.